Analyst

PAPER

View Article Online
View Journal | View Issue

Cite this: *Analyst*, 2023, **148**, 5144

Graphene-enhanced quantum cascade laser infrared spectroscopy using diamond thin-film waveguides

Andrea Teuber, [a] Giada Caniglia,[a] Christine Kranz [a] and Boris Mizaikoff *[a,b]

Received 23rd May 2023,
Accepted 4th September 2023

DOI: 10.1039/d3an00824j

rsc.li/analyst

Diamond thin-film waveguides were combined with quantum cascade lasers augmented by drop-casted graphene enabling surface-enhanced infrared absorption spectroscopy. Enhancing the signal provides access to an even more pronounced vibrational signature suitable for analytical scenarios where only a small sample volume and/or low analyte concentration levels are prevalent. To demonstrate the utility of this concept, taurine was investigated as a model analyte.

1. Introduction

The mid-infrared (MIR) spectroscopy is a well-known technique, which is non-destructive and operates in the spectral window of 4000–400 cm^{-1} (5–25 μm). The specificity of such so-called 'fingerprint spectra' renders MIR spectroscopy ideally suited for the selective and sensitive identification and quantification of molecular species.[1,2] MIR spectroscopic systems in general comprise a light source, a transducer, and a detector along with a data pre-processing unit. In conventional Fourier-transform infrared (FT-IR) devices, broad-band black body radiation is commonly used emitting across the entire MIR band. The radiation is modulated *via* an interferometer, and the time domain signal is transformed into the frequency domain *via* a Fourier transformation.[2–5] If a higher energy density per wavelength is needed, laser spectroscopy is a viable alternative. In that respect, interband and quantum cascade lasers (ICLs, QCLs) have revolutionized MIR spectroscopy in the past 25 years providing laser emission between 3 μm and 25 μm. When coupled to external cavities, tuning ranges across several hundreds of wavenumbers are achieved while combining the molecular selectivity inherent to the MIR regime with exceptional energy densities within the provided spectral window.[5–7] As the active sensing interface/transducer, a variety of sampling accessories can be selected,[8] whereby the reproducible interaction of photons and with the analyte of interest has to be ensured.[9] For liquids, semi-solids (*e.g.*, gels, pastes, *etc.*), and solids, attenuated total reflection (ATR) spectroscopy provides the ideal sensing configuration. With the photon-sample interaction inherently limited by the penetration depth of the evanescent field (*i.e.*, few micrometers), ATR spectroscopy may even be used for highly IR-opaque matrices, *e.g.*, water.[10] A wide range of IR-transparent waveguide materials may be used as the internal reflection element (IRE) or with diamond providing exceptional chemical inertness, biocompatibility, and transparency.[11] In general, suitable waveguide materials need to provide a refractive index higher than the sample such that the radiation may propagate inside the waveguide *via* total internal reflection at or below the critical angle. At the interaction interface with the optically less dense medium (*i.e.*, sample) *vs.* the reflection element, an evanescent field is prevalent, which penetrates exponentially decaying into the low refractive index sample medium. The penetration depth is a function of the wavelength, the angle of incidence, and the refractive index contrast between the waveguide and the adjacent medium.[12–14] The number of internal reflections is dependent on the length and geometric properties of the IRE with macroscopic waveguides providing discrete evanescent field hotspots where the sample may absorb IR radiation at resonant wavelengths. Thereby, the radiation at this wavelength is attenuated leading to an evanescent field absorption spectrum, which follows a quantitative pseudo-Lambert–Beer relationship. By reducing the geometrical dimensions of the waveguide, the intensity of the evanescent field and therefore the achievable signal-to-noise-ratio (SNR) can be increased achieving single-mode waveguiding behavior once the waveguide thickness approaches the order of magnitude of the propagating wavelength. Thereby, a continuous evanescent field is generated in contrast to discrete hotspots at macroscopic IREs.[15–20]

While MIR spectra may exhibit low sensitivity due to weak molecular absorption cross-sections or because of dilute solutions, metallic nanostructures may serve as signal amplifiers *via*

[a]*Institute of Analytical and Bioanalytical Chemistry, University of Ulm, 89081 Ulm, Germany. E-mail: boris.mizaikoff@uni-ulm.de*
[b]*Hahn-Schickard, 89077 Ulm, Germany*

pronounced electromagnetic near-field confinement and associated enhancement effects. This approach is termed SEIRA (surface-enhanced infrared absorption) spectroscopy,[21–23] which was first described by Hartstein *et al.*[24] The effect of enhancing IR spectra is based on field/antenna effects as well as the coupling on molecular vibrations with plasmonic resonances as apparent in, *e.g.*, gold (Au) and silver (Ag) nanoparticles (NPs).[22,25] Surface plasmons are charge oscillations at the metal-dielectric medium interface, which give rise to pronounced localized fields, which may couple with vibrations of molecules/analyte adsorbed or in close (*i.e.*, few molecular radii) distance to the metal surface. Such local fields and traveling surface waves (surface *i.e.*, polaritons)[26] may lead to IR signal enhancements by several orders of magnitude.[23,27] Frequently Au and Ag NP islands at a waveguide surface are used as amplifying sample interfaces.[26,28] However, such structures have a limited utility, as they do not allow a uniform enhancement across a broad spectral window given the weak field confinement and the limited tuneability (*i.e.*, resonant frequencies can be adjusted by the geometrical size of the nanostructures/antennas).[23,29]

To circumvent this disadvantage, graphene has been introduced as a surface-enhancing material owing to its unique properties, which have led to the introduction of so-called GEIRA (graphene-enhanced infrared absorption) spectroscopy.[22,29]

Graphene is a 2-dimensional (2D) semi-metallic material with sp^2-bonded carbons arranged in a honeycomb pattern. It is chemically inert and mechanically flexible and binds non-covalently to (bio) molecules. Graphene also provides spatially tight plasmon confinement and an extended plasmon propagation distance.[29] Graphene plasmons are therefore characterized by a pronounced light–matter interaction, plasmon resonances in the MIR range, a long plasmon lifetime, and a high degree of confinement. Graphene (nano)antennas have unprecedented field confinement and produce localized fields in the MIR range with modes beyond the excitation wavelength.[23,25,27,30] Single-layer graphene has relatively weak plasmonic resonances due to impurities and defects induced during its growth, has a reduced plasmon lifetime and no effective light-plasmon interaction occurs. Graphene multilayers instead have a strong plasmonic response and light–matter interactions.[31]

Coupling infrared attenuated total reflection (IR-ATR) spectroscopy with GEIRA provides access to highly confined graphene plasmons enhancing molecular IR absorptions in aqueous solutions. Graphene also suppresses the spectral signal from bulk water, as it reduces the evanescent field penetration depth leading to a decrease in water interference.[23,27,32] The ATR waveguide surface serves as a supporting substrate for the deposition of such signal-enhancing nanomaterials,[29] which allows for the nondestructive and label-free sensing of exceedingly low analyte concentrations.[27] Indeed, to date only a few IR sensors taking advantage of GEIRA have been reported.[23]

Proteins are important for human well-being. For example, the aggregation of specific proteins – and potentially involved secondary structure or conformation changes – can be associated with neurodegenerative disorders such as Alzheimer's and Parkinson's disease.[33] Understanding the disease mechanism – and underlying molecular changes – is pivotal to the disease diagnosis and potential therapeutic strategies. Taurine is an exemplary molecule that has beneficial effects on neurological diseases as a protein stabilizer due to its antioxidant effects. Taurine is among the most abundant amino acids in mammals and considered an essential nutrient for humans found at high concentrations in the heart and muscles,[34] and does not participate in peptide bonding.[35] Taurine is consumed in the daily diet (*e.g.*, meat, seafood, milk),[36] but also serves as a commonly used supplement (*e.g.*, in energy drinks).

Herein, we report an infrared laser-spectroscopic concept for the first time combining GEIRA with the benefits of thin-film diamond waveguides providing sufficient signal amplification for detecting the model analyte taurine at relevant concentration levels for supplements with an up to 20-fold enhancement of its characteristic IR signature.

2. Experimental

2.1 Optical setup

The optical setup shown in Fig. 1 comprises a thin-film diamond waveguide chip (TFWG; 5 × 10 mm^2, $w \times l$; waveguide layer thickness: 20 μm C) serving as an ATR waveguide mounted into a MIRaGuide (MG Optical Solutions GmbH, Germany) assembly aligned *via* an *x*–*y*–*z* stage (Newport, MKS instrument INC., USA). As a light source, a water-cooled external cavity QCL tunable in the region 1754–1493 cm^{-1} (MIRcat, DRS, Daylight Solutions, USA) has been used. The spectra were recorded in the range of 1680–1580 cm^{-1} with a spectral resolution of 2 cm^{-1}. The laser radiation was focused *via* ZnSe lenses (Thorlabs Inc., USA) onto the TFWG and then onto the detector, which was a 4-stage TE-cooled MCT device (PVI-4TE-10.6/MIP-10-1M-F-M4, Vigo System S.A., Poland).

2.2 Data treatment (laser spectra)

The laser spectra were collected *via* a custom LabView-based GUI (National Instrument Corp., Austin, USA), and digitized *via* an AD/DA card (NI-DAQmx, National Instruments Corp., USA). Each taurine sample (30 μL of aqueous solution) was analyzed nine times. For each measurement, an aliquot had been applied onto the sensing element leading to nine individual spectra that were then averaged. The data were imported into Origin (Origin Lab 2019b, USA) and a 3-point FFT filter was applied followed by averaging the data. The background measurement was pure water.

2.3 Data treatment (FT-IR spectra)

To verify the laser spectra of taurine comparison studies *via* conventional FT-IR spectroscopy using a single-bounce diamond ATR assembly (Alpha FT-IR with Platinum ATR; both Bruker, Germany) was used. 30 μL of each sample were ana-

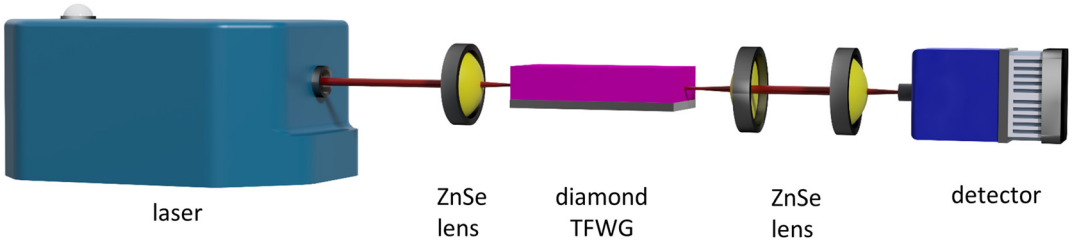

Fig. 1 Schematic of the QCL-based sensing system. The MIR laser beam is focused onto the front facet of the diamond thin-film waveguide; at the distal end, two lenses focus the emanating radiation onto the detector.

lyzed three times at a spectral resolution of 2 cm^{-1} collecting 128 scans and averaged using a 7- and 13-point FFT filter *via* Origin (OriginLab 2019b, USA). RedBull (RedBull, Austria) and RedBull 0 sugar (RedBull, Austria) cans were opened freshly for taurine measurement on both, the laser-based device and the FT-IR system.

2.4 Sample preparation for GEIRA studies

For GEIRA studies, a solution of 1 mg mL^{-1} graphene in DMF was purchased from Sigma Aldrich (Germany). According to the manufacturer, the graphene flakes have a thickness (80% of probability) of 1–3 layers of graphene corresponding (with approx. 0.5 nm thickness per layer)[37] and an oxygen content of 7.5% (C/O ratio: 12.3). The graphene preparation was performed *via* electrochemical exfoliation. 1 mg mL^{-1} graphene in DMF was diluted to a 0.05 w/w% with ethanol based on literature,[29] and ultra-sonicated. In ref. 29, preliminary tests with graphene were conducted suggesting that dried graphene at the waveguide surface reveals higher enhancement factors compared to graphene flakes remaining immersed in liquid. Therefore, 1.5 μL of the graphene dispersion was drop-coated onto the waveguide and dried. 0.4 w/w% taurine solutions were freshly prepared with MilliQ water (18.0 MO cm, Elga Labwater; VWS, Deutschland, Germany), and 30 μL aliquots were applied onto the graphene-modified diamond surface. After the analysis, the solution was removed with an Eppendorf pipette, the waveguide surface was cleaned several times with water (no tissue was used) and another layer of graphene was drop-coated, dried, and again taurine solution was applied.

2.5 AFM and SEM studies

AFM measurements were performed using a 5500 AFM/SPM microscope (Keysight Technologies, AZ, USA). The AFM images were recorded in air in contact mode using a silicon probe (RTESPA-300, Bruker AFM probes, CA, USA; nominal frequency of 300 kHz) at a scan speed of 0.60 ln s^{-1}. Surface analyses were evaluated using MoutainSPIP v.9 (Digital Surf, France). The SEM images were acquired using a Helios Nanolab 600 FIB/SEM system (ThermoFisher, the Netherlands) at 3.00 kV and a beam current of 86 pA.

3. Results and discussion

3.1 Graphene flakes analyzed *via* AFM and SEM

AFM and SEM studies were performed investigating the graphene flakes dispersed at a silicon wafer surface, which were prepared using the same procedure for deposition at the diamond TFWG. The benefit of using a silicon surface for SEM experiments is the higher achievable contrast given the nature of the diamond, which may affect the imaging quality due to charge effects.

In Fig. 2A and B AFM images are shown, while Fig. 2C and D provide SEM images of graphene drop-coated onto the silicon wafer. The SEM images indicate graphene islands or graphene flakes dispersed along the surface. High-resolution AFM images allow studying more detailed topographical features of the graphene islands. Evidently, the graphene coating is responsible for an increased roughness *vs.* the graphene islands and 0.062 ± 2 nm (n = 4) for the uncoated surface with a root-mean-square roughness (S) derived from the AFM

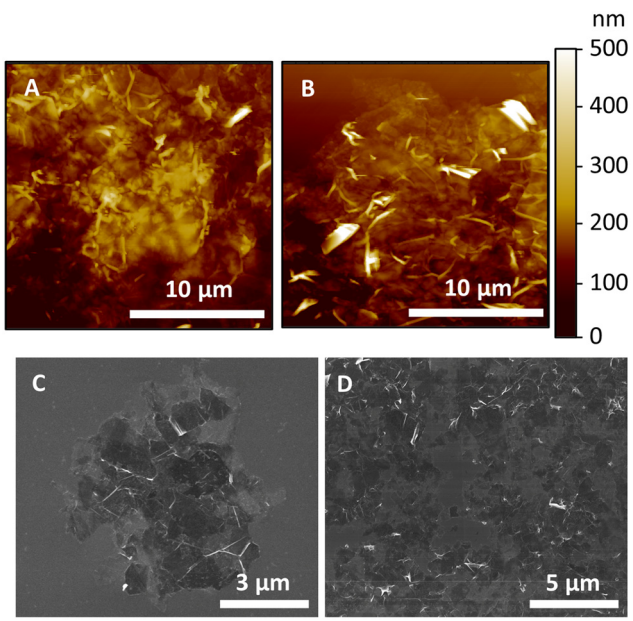

Fig. 2 AFM (A and B) and SEM (C and D) images of graphene drop-coated onto a silicon wafer surface.

images as 0.86 ± 0.02 nm (n = 4) for wafer bare surface (roughness has been calculated from 5 × 5 μm^2 AFM images). According to the literature, the thickness of a graphene layer is approx. 0.5 nm and the interlayer distance between adjacent graphene layers is equal to approx. 0.33 nm.[37,38] With these parameters, it was possible to estimate the number of graphene layers after drop-coating *via* AFM imaging at approx. 13 ± 2 nm (n = 4), which corresponds to approx. 14–19 layers of graphene translating into multilayer graphene islands.

3.2 Taurine studies *via* conventional IR-ATR and QCL-TFWG

Using conventional IR-ATR spectroscopy, characteristic spectra of taurine were recorded (Fig. 3) for reference. 0.4 w/w% of taurine was selected, as this is the concentration of taurine reported for energy drinks, herein, RedBull (Redbull, Austria). Therefore, 0.4 w/w% of taurine aqueous solution, as well as RedBull and RedBull 0 sugar have been analyzed *via* conventional IR-ATR and QCL-TFWG spectroscopy, as compared in Fig. 3B (IR-ATR) and Fig. 3C (QCL). The ingredients of RedBull were collected as supplied on the label (water, sucrose, glucose, acidifier (citric acid), carbonic acid, taurine (0.4%), acidity regulators (sodium carbonates, magnesium carbonates), caffeine (0.3%), vitamins (niacin, pantothenic acid, B6, B12), flavors, colorants (caramel, riboflavins)). Comparing the main ingredients of the RedBull with its characteristic IR signature in the applied spectral region (1660–1580 cm^{-1}) reveals that sucrose, glucose, citric acid, sodium, and magnesium carbonate have no significant vibrational signatures in this regime.[39]

Other constituents, *i.e.*, niacin, pantothenic acid, B6, B12, caramel, and riboflavins indeed show vibrational characteristics in this range. However, since they are present at exceedingly low concentrations (<0.3 w/w%), their influence on determining the main component taurine in that spectral window was considered negligible and no comprehensive interpretation of their spectral contributions was performed. While a more detailed analysis of all minor ingredients was not the aim of the present investigation, detailed investigation for the

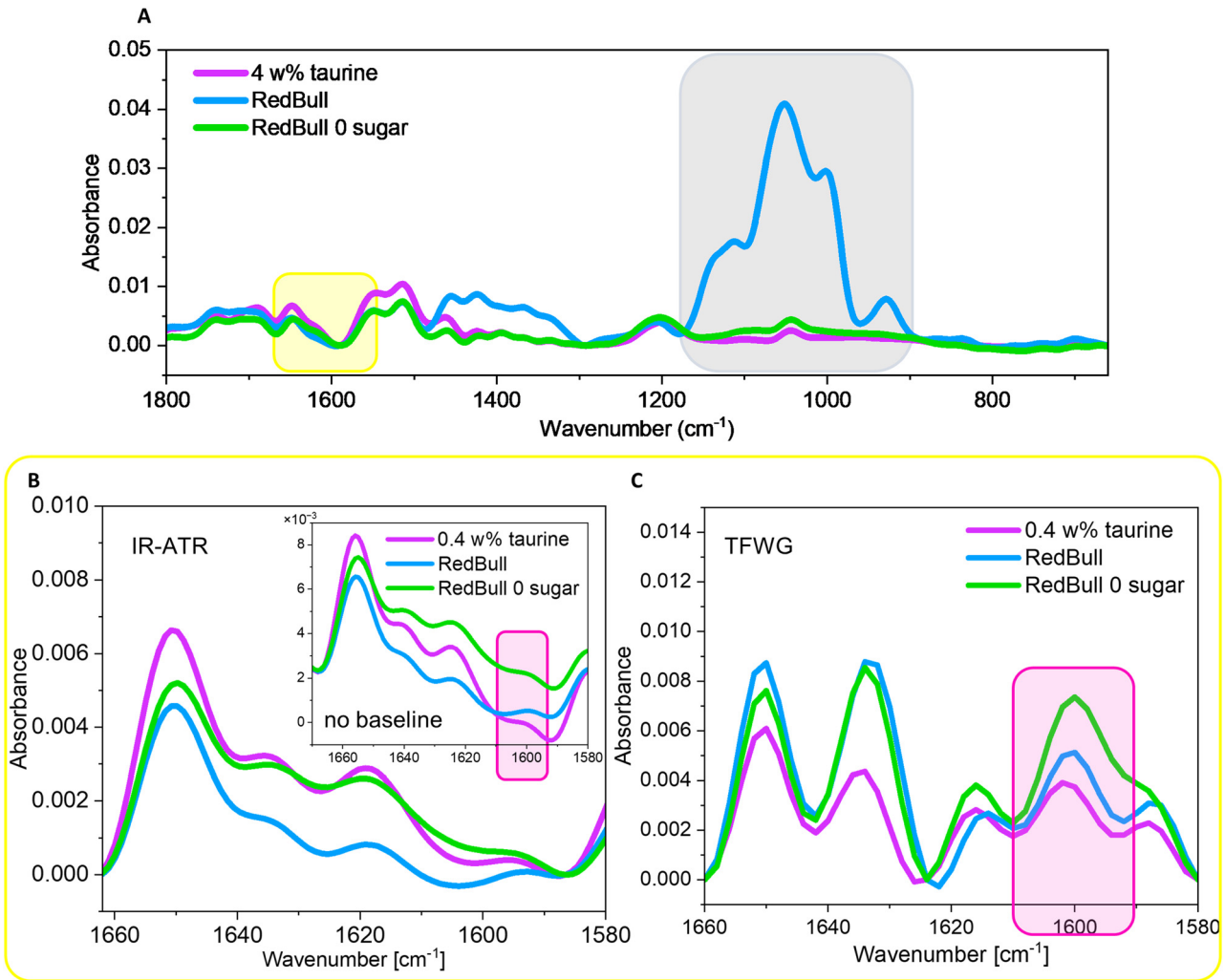

Fig. 3 (A) IR-ATR spectrum shows the range between 1800 cm^{-1} and 600 cm^{-1} with its characteristic vibrations (inset: IR-ATR spectrum without baseline correction). (B) IR-ATR and (C) laser-based spectra in the Amide I range.

compounds, as in previous study has focused on additional components such as caffein using QCL-based IR-ATR spectroscopy.[40] Sucrose and glucose are apparently not interfering in the wavelength regime of interest between 1660 cm^{-1} and 1580 cm^{-1}, as evident from the RedBull 0 spectra (Fig. 3A) where the sample contains no sugars at all. The same samples (RedBull, RedBull 0 sugar, 0.4 w/w% aqueous taurine solution) were then analyzed with the QCL-TFWG system. For comparison, Fig. 3A shows the IR spectrum (with baseline correction at 1976 cm^{-1}, 1590 cm^{-1}, 1295 cm^{-1}, and 656 cm^{-1}) recorded with an FT-IR and conventional ATR assembly across the relevant spectral range, *i.e.*, between 1800 cm^{-1} and 600 cm^{-1}. A characteristic vibrational band of taurine is the SO-vibration at around 1205 cm^{-1}, 1033 cm^{-1}, and 1020 cm^{-1} (see grey box; with overlapping glucose/sucrose signatures).[41]

The yellow box in Fig. 3A indicates the wavelength range selected for evaluating the vibrational signature of taurine. Fig. 3B shows the IR spectrum recorded with conventional FT-IR in the relevant spectral range and Fig. 3C the corresponding QCL-based spectrum (compare with yellow box in Fig. 3A). A baseline correction has been individually applied for the FT-IR spectrum (1664 cm^{-1} and 1587 cm^{-1}) and for the laser-based spectrum (1660 cm^{-1}, 1624 cm^{-1} and 1580 cm^{-1}). It is worth mentioning that the peak at around 1600 cm^{-1}, which corresponds to the NH_2 vibration (see Table 1) when analyzed *via* IR-ATR is a rather weak signature (see inset without baseline correction). Evidently, this peak may shift within the spectrum. Both experiments confirm the utility of IR-spectroscopy for analyzing taurine in an energy drink matrix. When comparing the FT-IR-based spectrum (Fig. 3B) with the laser-based spectrum (Fig. 3C), much more pronounced vibrational features are evident when using the QCL providing significantly more pronounced IR spectra. An assignment of the vibrational features of taurine in the amide region (1660–1580 cm^{-1}) is given in Table 1 based on literature values. Apparently, most signatures in the literature are assigned using conventional IR-ATR spectra with some features only evident using the present combination of tunable QCL and diamond TFWG.

3.3 GEIRA and laser-based IR spectroscopy of taurine

After the suitability of analyzing taurine using a pristine diamond TFWG was confirmed, graphene flakes were used to enhance the signal of laser-based IR spectra based on the GEIRA principle. Although it is for sure also interesting to investigate the enhancement behavior of conventional IR-ATR techniques, similar studies were already shown before. For example, Hu *et al.*[29] demonstrated that dried graphene flakes at an IRE surface provide a more pronounced GEIRA effect *vs.* graphene dispersed in a sample solution. Furthermore, different model analytes including auramine, crystal violet, fuchsine, methylene blue, neutral red, and rhodamine B were readily analyzed with and without graphene.[29] Since these analytes revealed a significant enhancement effect for the amide I band, taurine was anticipated to exhibit a similar enhancement factor when analyzed *via* QCL-based IR-ATR spectroscopy

Table 1 Assignment of vibrational features of taurine in the amide I range and correlated functional groups

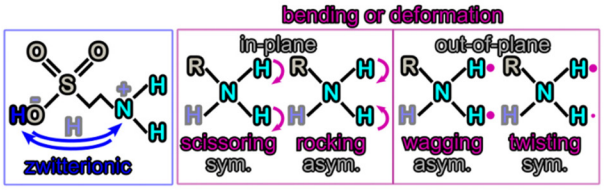

	NH s	amide		NH_2 s			
	NH_3 b	NH_2 s	NH_3 b	NH_3 a, b	NH_2	NH_3 a, b	Ref
Powder[A]				1616		1585	(41)
SEIRA[A]				1614		1583	(41)
FT-IR[A]	1654		1625				(42)
Solid (X)				1651		1585	(43)
Calc. (X)				1620 1618			(43)
Solid (Y)		1641					(43)
Calc. (Y)				1621			(43)
FT-IR[A]	1650 – 1550						(44)
FT-IR					1600		(36)
FT-IR		1638					(45)
FT-IR	1651	1635		1619	1595		This work
Diamond	1650	1634		1616	1602	1588	
GEIRA 1x	1650	1634		1616		1584	
GEIRA 2x	1650	1634		1612	1594		
GEIRA 3x	1650	1634	1620	1612	1594		

Abbreviations: Calc. = calculated, X: pH = 4.8, Y: pH = 10.3, a = asymmetric deformation, b = bending, s = scissoring; A = ATR measurement.

augmented by drop-coated graphene flakes at the surface of diamond TFWGs.

Fig. 4 shows the corresponding IR spectra recorded first at the pristine diamond TFWG, and then after modification with graphene. For the spectra shown in Fig. 4, no baseline correction was applied. It was also tested whether adding additional layers of graphene (up to 3 times) results in an additional enhancement effect. After depositing a layer of graphene flakes, a distinct enhancement effect is evident, which increases with the deposition of a second graphene layer. As shown in Fig. 2, the drop-casting/drying procedure yields an inhomogeneous graphene layer with increased coverage after further deposition cycles. After depositing the third layer of graphene flakes, the already quite pronounced enhancement effect only minutely increases, which is associated with full coverage of the waveguide surface. Considering the enhancement factor (EF) as the ratio between the intensity of the analyte in GEIRA-based spectra *vs.* the intensity of characteristic spectral signatures recorded at the pristine diamond surface, an EF of approx. 20 was observed in selected spectral regions,[29] of which are in accordance with previous studies.[29]

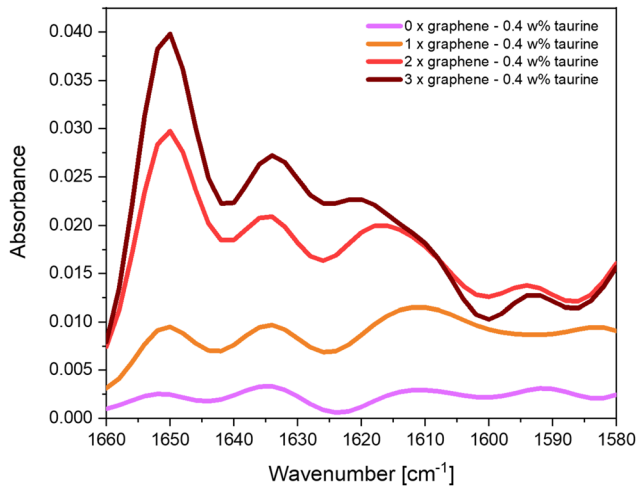

Fig. 4 Graphene surface-enhanced infrared absorption (GEIRA) spectroscopy *via* diamond TFWGs and QCL laser spectroscopy. Increasingly enhanced taurine spectra (0.4 w% in water) were recorded at the pristine diamond TFWG surface and after the deposition of 1–3 layers of graphene flakes.

To investigate the influence of graphene on the taurine spectrum, the first pristine diamond TFWG spectrum was recorded followed by taurine at 1–3 deposited layers of graphene, respectively. It was confirmed that using graphene significantly enhances the vibrational features characteristic of taurine without causing any spectral shifts.[42]

4. Conclusion

Herein, we combine diamond thin-film waveguides with laser-based mid-infrared spectroscopy and graphene for surface-enhanced spectroscopy for the first time. As an exemplary analyte, taurine was investigated at a concentration relevant to the determination of energy drinks. Comparing the obtained IR spectra with conventional IR-ATR spectroscopy confirms that the proposed sensing concept using GEIRA provides an up to 20-fold signal enhancement rendering the system useful for future applications in beverage quality analysis and control. In particular, diamond thin-film waveguides are exceedingly robust sensing interfaces readily renewable *via* drop-casted graphene layers probing only minute sample quantities. Finally, the latter aspect along with the obtained signal enhancement renders this sensing platform ideally suited for biomedical assays that usually require addressing low concentrations in small volumes.

Author contributions

All authors have approved the final version of the manuscript. Andrea Teuber: conceptualization, experiments, data curation, writing – original draft, writing – review & editing; Giada Caniglia: data curation of AFM; Christine Kranz and Boris Mizaikoff: supervision, writing – review & editing.

Conflicts of interest

There are no conflicts to declare.

Acknowledgements

This work has been supported by the BMBF project "GRA//DIA - Graphen-auf-Bor-dotiertem-Diamant: Markierungsfreie Bioassays mittels oberflächenverstärkter Infrarot-Spektro-elektrochemie" (#03XP0206B).

We thank Dr Gregor Neusser at the Focused Ion Beam Center UUlm (Institute of Analytical and Bioanalytical Chemistry, Ulm University) for assistance with the SEM studies.

References

1 J. Haas and B. Mizaikoff, Advances in Mid-Infrared Spectroscopy for Chemical Analysis, *Annu. Rev. Anal. Chem.*, 2016, **9**, 45–68.
2 L. Hvozdara, N. Pennington, M. Kraft, M. Karlowatz and B. Mizaikoff, Quantum cascade lasers for mid-infrared spectroscopy, *Vib. Spectrosc.*, 2002, **30**(1), 53–58.
3 P. R. Griffiths, Fourier Transform Infrared Spectrometry, *Science*, 1983, **222**(4621), 297–302.
4 T. G. Mayerhöfer, S. Pahlow and J. Popp, Recent technological and scientific developments concerning the use of infrared spectroscopy for point-of-care applications, *Spectrochim. Acta, Part A*, 2021, **251**, 119411.
5 A. Teuber and B. Mizaikoff, Cascade Laser Infrared Spectroscopy, in *Encyclopedia of Analytical Chemistry*, Wiley, 2021, pp. 1–45.
6 J. Haas, E. V. Catalán, P. Piron, M. Karlsson and B. Mizaikoff, Infrared spectroscopy based on broadly tunable quantum cascade lasers and polycrystalline diamond waveguides, *Analyst*, 2018, **143**(21), 5112–5119.
7 A. Teuber, R. Stach, J. Haas and B. Mizaikoff, Innovative Substrate-Integrated Hollow Waveguide Coupled Attenuated Total Reflection Sensors for Quantum Cascade Laser Based Infrared Spectroscopy in Harsh Environments, *Appl. Spectrosc.*, 2022, **76**(1), 132–140.
8 T. Schädle and B. Mizaikoff, Mid-Infrared Waveguides: A Perspective, *Appl. Spectrosc.*, 2016, **70**(10), 1625–1638.
9 T. Schädle and B. Mizaikoff, Selecting the Right Tool: Comparison of the Analytical Performance of Infrared Attenuated Total Reflection Accessories, *Appl. Spectrosc.*, 2016, **70**(6), 1072–1079.
10 A. Teuber and B. Mizaikoff, RobustATR: Substrate-Integrated Hollow Waveguide Coupled Infrared Attenuated Total Reflectance Sensors, *Appl. Sci.*, 2022, **12**(19), 10019.

11 M. Malmström, M. Karlsson, P. Forsberg, Y. Cai, F. Nikolajeff and F. Laurell, Waveguides in polycrystalline diamond for mid-IR sensing, *Opt. Mater. Express*, 2016, **6**(4), 1286.
12 N. J. Harrick, Study of Physics and Chemistry of Surfaces from Frustrated Total Internal Reflections, *Phys. Rev. Lett.*, 1960, **4**(5), 224–226.
13 M. Milosevic, On the Nature of the Evanescent Wave, *Appl. Spectrosc.*, 2013, **67**(2), 126–131.
14 M. Milosevic, Internal Reflection and ATR Spectroscopy, *Appl. Spectrosc. Rev.*, 2004, **39**(3), 365–384.
15 Á.I López-Lorente, M. Karlsson, L. Österlund and B. Mizaikoff, Diamond Waveguides for Infrared Spectroscopy and Sensing, in *Carbon-Based Nanosensor Technology*, ed. C. Kranz, Springer International Publishing, Cham, 2019, pp. 87–117.
16 J. Haas, E. V. Catalán, P. Piron, F. Nikolajeff, L. Österlund, M. Karlsson, *et al.*, Polycrystalline Diamond Thin-Film Waveguides for Mid-Infrared Evanescent Field Sensors, *ACS Omega*, 2018, **3**(6), 6190–6198.
17 X. Wang, M. Karlsson, P. Forsberg, M. Sieger, F. Nikolajeff, L. Österlund, *et al.*, Diamonds are a spectroscopists best friend: Thin-film diamond mid-infrared waveguides for advanced chemical sensors/biosensors, *Anal. Chem.*, 2014, **86**(16), 8136–8141.
18 P. Piron, E. Vargas Catalan, F. Nikolajeff, L. Österlund, P. O. Andersson, J. Bergström, *et al.*, Development of a diamond waveguide sensor for sensitive protein analysis using IR quantum cascade lasers, *Proc. SPIE*, 2018, **10539**(105390F-1), 15.
19 X. Wang, S. S. Kim, R. Roßbach, M. Jetter, P. Michler and B. Mizaikoff, Ultra-sensitive mid-infrared evanescent field sensors combining thin-film strip waveguides with quantum cascade lasers, *Analyst*, 2012, **137**(10), 2322–2327.
20 P. Forsberg, P. Hollman and M. Karlsson, High sensitivity infrared spectroscopy with a diamond waveguide on aluminium nitride, *Analyst*, 2021, **146**(22), 6981–6989.
21 Y. Cai, Y. Hang, Y. Zhou, J. Zhu, J. Yang and X. Wang, Graphene-Based Biosensors for Detection of Composite Vibrational Fingerprints in the Mid-Infrared Region, *Nanomaterials*, 2019, **9**(10), 1496.
22 J. Nong, L. Tang, G. Lan, P. Luo, Z. Li, D. Huang, *et al.*, Enhanced Graphene Plasmonic Mode Energy for Highly Sensitive Molecular Fingerprint Retrieval, *Laser Photonics Rev.*, 2021, **15**(1), 2000300.
23 B. Zheng, X. Yang, J. Li, C. F. Shi, Z. L. Wang and X. H. Xia, Graphene Plasmon-Enhanced IR Biosensing for in Situ Detection of Aqueous-Phase Molecules with an Attenuated Total Reflection Mode, *Anal. Chem.*, 2018, **90**(18), 10786–10794.
24 A. Hartstein, J. R. Kirtley and J. C. Tsang, Enhancement of the Infrared Absorption from Molecular Monolayers with Thin Metal Overlayers, *Phys. Rev. Lett.*, 1980, **45**(3), 201–204.
25 J. Nong, L. Tang, G. Lan, P. Luo, Z. Li, D. Huang, *et al.*, Combined Visible Plasmons of Ag Nanoparticles and Infrared Plasmons of Graphene Nanoribbons for High–Performance Surface–Enhanced Raman and Infrared Spectroscopies, *Small*, 2021, **17**(1), 2004640.
26 P. R. Griffiths, Surface-enhanced infrared absorption spectroscopy: principles and applications, in *Spectrosc. Prop. Inorg. Organomet. Compd*, 2013, vol. 44, pp. 95–122.
27 F. Cao, L. Wu, Y. Ruan, J. Bai and X. Jiang, In Situ Surface-Enhanced Infrared Absorption Spectroscopy of Aqueous Molecules with Facile-Prepared Large-Area Reduced Graphene Oxide Island Film, *Anal. Chem.*, 2018, **90**(11), 6526–6531.
28 Y. Francescato, V. Giannini, J. Yang, M. Huang and S. A. Maier, Graphene Sandwiches as a Platform for Broadband Molecular Spectroscopy, *ACS Photonics*, 2014, **1**(5), 437–443.
29 Y. Hu, Á. I. López-Lorente and B. Mizaikoff, Versatile Analytical Platform Based on Graphene-Enhanced Infrared Attenuated Total Reflection Spectroscopy, *ACS Photonics*, 2018, **5**(6), 2160–2167.
30 H. Hu, X. Guo, D. Hu, Z. Sun, X. Yang and Q. Dai, Flexible and Electrically Tunable Plasmons in Graphene-Mica Heterostructures, *Adv. Sci.*, 2018, **5**(8), 1800175.
31 Q. Guo, C. Li, B. Deng, S. Yuan, F. Guinea and F. Xia, Infrared Nanophotonics Based on Graphene Plasmonics, *ACS Photonics*, 2017, **4**(12), 2989–2999.
32 C. Wu, X. Guo, Y. Duan, W. Lyu, H. Hu, D. Hu, *et al.*, Ultrasensitive Mid–Infrared Biosensing in Aqueous Solutions with Graphene Plasmons, *Adv. Mater.*, 2022, **34**(27), 2110525, DOI: **10.1002/adma.202110525**.
33 V. Mittal, G. Devitt, M. Nedeljkovic, L. G. Carpenter, H. M. H. Chong, J. S. Wilkinson, *et al.*, Ge on Si waveguide mid-infrared absorption spectroscopy of proteins and their aggregates, *Biomed. Opt. Express*, 2020, **11**(8), 4714.
34 M. A. Bhat, K. Ahmad, M. S. A. Khan, M. A. Bhat, A. Almatroudi, S. Rahman, *et al.*, Expedition into Taurine Biology: Structural Insights and Therapeutic Perspective of Taurine in Neurodegenerative Diseases, *Biomolecules*, 2020, **10**(6), 863.
35 S. W. Schaffer, C. Ju Jong, K. C. Ramila and J. Azuma, Physiological roles of taurine in heart and muscle, *J. Biomed. Sci.*, 2010, **17**(Suppl 1), S2.
36 S. Triebel, C. Sproll, H. Reusch, R. Godelmann and D. W. Lachenmeier, Rapid analysis of taurine in energy drinks using amino acid analyzer and Fourier transform infrared (FTIR) spectroscopy as basis for toxicological evaluation, *Amino Acids*, 2007, **33**(3), 451–457.
37 V. Kumar, A. Kumar, D. J. Lee and S. S. Park, Estimation of Number of Graphene Layers Using Different Methods: A Focused Review, *Materials*, 2021, **14**(16), 4590.
38 S. V. Morozov, K. S. Novoselov, F. Schedin, D. Jiang, A. A. Firsov and A. K. Geim, Two-dimensional electron and hole gases at the surface of graphite, *Phys. Rev. B: Condens. Matter Mater. Phys.*, 2005, **72**(20), 201401.
39 D. Siderius, *NIST Standard Reference Simulation Website - SRD 173*, National Institute of Standards and Technology, 2017.

40 A. Teuber, G. Caniglia, M. Wild, M. Godejohann, C. Kranz and B. Mizaikoff, Espresso Science: Laser-Based Diamond Thin-Film Waveguide Sensors for the Quantification of Caffeine, *ACS Sens.*, 2023, **8**, 1871–1881.

41 N. Kumar, S. Thomas, R. B. Tokas and R. J. Kshirsagar, Investigation on the adsorption characteristics of sodium benzoate and taurine on gold nanoparticle film by ATR–FTIR spectroscopy, *Spectrochim. Acta, Part A*, 2014, **118**, 614–618.

42 P. Bruździak, A. Panuszko, E. Kaczkowska, B. Piotrowski, A. Daghir, S. Demkowicz, *et al.*, Taurine as a water structure breaker and protein stabilizer, *Amino Acids*, 2018, **50**(1), 125–140.

43 K. Ohno, Y. Mandai and H. Matsuura, Vibrational spectra and molecular conformation of taurine and its related compounds, *J. Mol. Struct.*, 1992, **268**(1–3), 41–50.

44 M. González-Vázquez, O. G. Meza-Márquez, T. Gallardo-Velázquez, G. Osorio-Revilla, J. L. Velázquez Hernández and M. Hernández-Martínez, Simultaneous Determination of Caffeine and Taurine in Energy Drinks by FT-MIR Spectroscopy Coupled with Multivariate Analysis, Camara JS, editor, *J. Spectrosc.*, 2020, **2020**, 1–7.

45 H. Pan, Y. Yu, L. Li, B. Liu and Y. Liu, Fabrication and Characterization of Taurine Functionalized Graphene Oxide with 5-Fluorouracil as Anticancer Drug Delivery Systems, *Nanoscale Res. Lett.*, 2021, **16**(1), 84.